Nanoscopic Porous Sensors

John J. Kasianowicz,[1] Joseph W.F. Robertson,[1] Elaine R. Chan,[1] Joseph E. Reiner,[1] and Vincent M. Stanford[2]

[1]National Institute of Standards and Technology, Semiconductor Electronics Division, Electronics and Electrical Engineering Laboratory, Gaithersburg, Maryland 20899-8120; email: john.kasianowicz@nist.gov

[2]National Institute of Standards and Technology, Information Access Division, Information Technology Laboratory, Gaithersburg, Maryland 20899-8940

Annu. Rev. Anal. Chem. 2008. 1:737–66

The *Annual Review of Analytical Chemistry* is online at anchem.annualreviews.org

This article's doi:
10.1146/annurev.anchem.1.031207.112818

1936-1327/08/0719-0737$20.00

Key Words

analyte detection, Coulter counter, DNA sequencing, ion channel, nanopore-based sensor, resistive-pulse detection

Abstract

There are thousands of different nanometer-scale pores in biology, many of which act as sensors for specific chemical agents. Recent work suggests that protein and solid-state nanopores have many potential uses in a wide variety of analytical applications. In this review we survey this field of research and discuss the prospects for advances that could be made in the near future.

1. INTRODUCTION

Nanopore chemical sensors are miniaturized descendents of the Coulter counter (1), a device that measures resistive pulses to detect microscopic particles, such as red blood cells, in a narrow capillary. The classical Coulter counter was able to detect ~10-μm-size particles in ~100-μm-diameter capillaries. These techniques were first applied to the nanoscale (~100 nm) with nuclear-track etched pores in the early 1970s by DeBlois and Bean (2). Other mesofluidic structures with diameters of less than 1 μm also have the potential for use in the analysis of macromolecules, colloids, and bioparticles measuring >100 nm (3–5).

Nanopore-based sensors are fundamentally chemical in nature because the interaction time of the analyte with the pore, when governed by physics alone, is too short to be accurately measured using electronics. Resistive-pulse techniques require an analyte to enter into and reside within a capillary for a period of time long enough to be detected with ionic current measurements. As resistive-pulse sensors are miniaturized to the molecular scale (1 to 10 nm), the characteristic diffusion time for a molecule becomes quite short (~50 to 500 ns), and only ~50 to 500 ions pass the molecule in a nanopore with a 1-nS conductance. For an analyte molecule to reside within the pore long enough for detection, there must be either an appreciable binding (or adsorption) of the analyte to the interior of the pore or a physical means to inhibit the partitioning of the analyte out of the pore. Therefore, optimizing the interfacial chemistry between an analyte and the nanopore interior must factor significantly into any successful detection scheme.

The first truly molecular-scale nanopores to be used experimentally were protein ion channels (**Figure 1*a***), the study of which formed the foundation of biophysics. Channels can selectively transport particular species of ions across cell membranes and alter their conductance state by changing the transmembrane electrostatic potential. By virtue of these two properties, channels form the molecular basis of many processes, including the propagation of neural impulses (6), muscle activity (7), and protein translocation across cell membranes (8, 9). More recent developments demonstrated that these nanodevices have the potential for use as chemical sensors.

The chemical affinity between protein ion channels embedded in planar lipid bilayer membranes and a variety of analytes has permitted the detection and quantification of H^+ and D^+ ions (10, 11), divalent cations (12, 13), single-stranded RNA and DNA molecules (14–19), small organic molecules (20), specific sugar molecules (21), poly(ethylene glycol) (PEG) (22–29), and anthrax toxins (30).

Whereas biological nanopores offer precisely controlled structures and interfacial chemistry, solid-state nanopores in silicon nitride have also been developed (**Figure 1*b***) (31–37) to take advantage of the potentially improved stability offered by semiconductor materials. Solid-state nanopores were initially used to detect individual double-stranded DNA (dsDNA) molecules (32), which are too large to transport through many ion channels (14). Other nanopores fabricated from carbon nanotubes (3) or by heavy ion bombardment combined with chemical etching (38, 39) have also made inroads into nanoscale pore sensor elements.

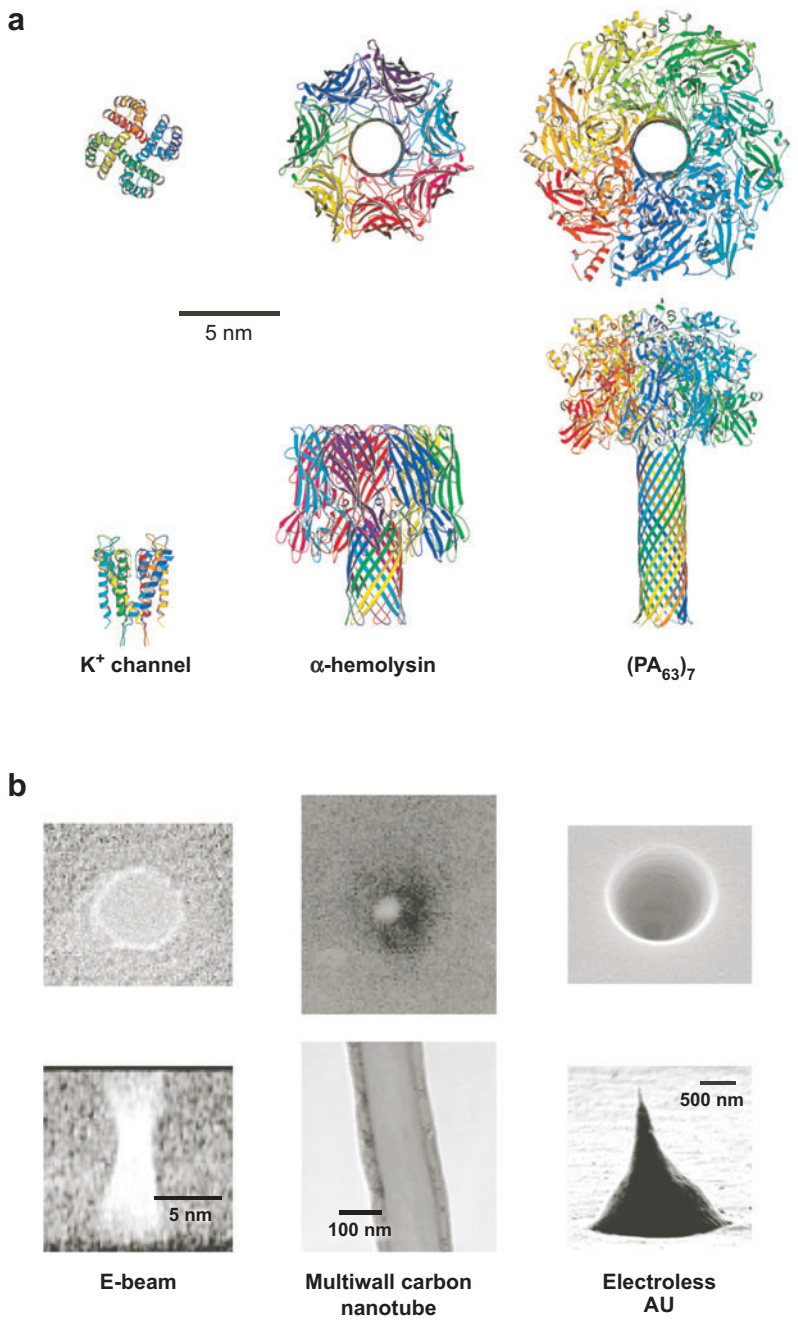

Figure 1

(*a*) Biological and (*b*) solid-state nanopores. (*a*) *From left to right*: crystal structures of a K^+-selective ion channel (118), and the channel formed by *Staphylococcus aureus* α-hemolysin (61) and a molecular model for the channel formed by *Bacillus anthracis* protective antigen 63 (119). (*b*) *From left to right*: synthetic silicon nitride nanopore (36), carbon multiwall nanotube in an epoxy matrix (3), and nanopores formed in track-etched polyimide, polycarbonate or poly(ethylene terephthalate) membranes (38, 39).

The experiments and theoretical methods described herein suggest that both protein and solid-state nanopores will continue to act as excellent platforms for single-molecule analytical measurements.

2. ELECTRONIC DETECTION OF MOLECULES USING SINGLE NANOMETER-SCALE PORES: SIGNAL PROCESSING

One advantage of the nanopore-based analyte detection method is that the resistive-pulse measurements are electronic. Thus, they have the potential to be performed at relatively low cost, and the resulting data are readily amenable to a wide variety of statistical signal processing algorithms.

Consider a model system consisting of a single nanopore in a high-impedance matrix. In the absence of analytes, the ionic current that flows through the pore in response to a fixed value of the applied potential is stable. Analytes that interact with the nanopore can alter the latter's conductance via electrostatic or steric interactions. Below, we identify three typical signals that are obtained in single-nanopore experiments and discuss the methods used to analyze the data.

2.1. Steady-State and Kinetic Analysis: Estimation of Event Amplitudes and Dwell Times

In the simplest case, the reversible interaction between an analyte and a single nanopore causes the pore conductance to fluctuate between two well-defined mean values. The analyte concentration can be determined by estimating the time spent by the nanopore in each of the two states, for instance via a conventional dwell-time approach (40–46). Because reaction kinetics are characteristic of the chemical interactions between analytes and a binding site, the dynamics of the current fluctuations also reveal information about the type of analyte.

At the extremes of analyte concentration (i.e., $[A] \ll K$ and $[A] \gg K$, where [A] is the analyte concentration, the binding constant of the reaction in mol/L is defined by $K = k_{off}/k_{on}$, and k_{on} and k_{off} are the rate constants for the association with and dissociation of analyte from the nanopore, respectively), the current will be virtually always in one state or the other (**Figure 2*a***, *left*). When the analyte concentration $[A] = K$, the channel spends, on average, half the time in each of the two conductance states. In a manner similar to the Henderson-Hasselbalch relation for the concentration of aqueous protons in a buffer solution, the time-averaged nanopore ionic current will vary monotonically from one extreme of the current to the other as a function of analyte concentration (**Figure 2*a***, *center*). Thus, calibration of a particular nanopore with known concentrations of an analyte enables the determination of the analyte concentration in a test solution (11).

The kinetics of the current fluctuations provide additional information to help determine the identity of the analyte. **Figure 2*a*** (*right*) illustrates two possible dwell-time distributions determined from two different hypothetical ionic current time series. If the reaction between the analyte and a nanopore can be described by a simple reversible chemical reaction, the lifetime distribution for events in the bound

state would be described by a single exponential. If the analyte concentration were low (i.e., [A] $\ll K$), the mean lifetime derived from the distribution would be $\sim 1/k_{off}$, which would be characteristic of the analyte type. For other types of interactions between the analyte and the nanopore (e.g., transport of analyte through the nanopore), the lifetime distribution may be better described by another function, such as a Gaussian.

2.2. Spectral Analysis

Fourier analysis has provided keen insight into the mechanism by which the neural impulse propagates across a synapse (47, 48), and is particularly useful for the analytical applications described herein for two reasons. First, it can be used to analyze current fluctuations that are not completely resolved due to bandwidth limitations (**Figure 2*b***, *left*). Second, it provides a direct measurement of the frequency content in the time series and hence of the characteristic timescales of the analyte-nanopore interactions.

For a random telegraph two-state system, the power spectral density (PSD) of the current noise is nearly white (i.e., frequency independent) at low frequencies; at higher frequencies, the PSD decreases as $1/f^2$ (49) (**Figure 2*b***, *center*, *blue trace)*. The transition between those two regimes is characterized by the corner frequency, f_c, which is the frequency at which the PSD decreases twofold. In general, f_c provides information about the two timescales of the reaction between the analyte and the nanopore: (1) the mean time the analyte is bound to the pore (obtained when [A] $\ll K$), and (2) the mean time the analyte takes to find and react with the nanopore (which depends on [A]) (50). For a given experiment, fitting a simple theoretical expression to an experimental PSD data set provides estimates for the low frequency noise, $S(0)$, and f_c (**Figure 2*b***, *center*, *black trace*).

As shown in **Figure 2*b*** (*right*, *blue trace*), at the extreme values of the analyte concentration, the value of $S(0)$ is minimal. For [A] $\approx K$, $S(0)$ approaches its maximum value. This makes intuitive sense: When there is a shortage or an excess of analyte, the current fluctuations must be minimal and the maximum of the current fluctuations must occur when the rates of analyte association with and dissociation from the pore are equal (11). The kinetic information in the reaction is determined from the characteristic relaxation time for the interaction between the analyte and the nanopore, defined as $\tau = 1/2\pi f_c$. In the limit of [A] ≈ 0, $\tau \sim 1/k_{off}$. For increasing values of [A], the second characteristic time of the reaction (related to k_{on} [A]) starts to dominate.

A least-squares fit of simple equations to the distributions of $S(0)$ and τ, derived from the PSD data as a function of analyte concentration, provides estimates for several reaction parameters, including the number of binding sites for analyte in the nanopore, the thermodynamic information about the reaction (i.e., the pK), and the kinetic information in terms of k_{on} and k_{off} (11, 24, 50). This method discriminates particularly well among the different analytes that bind to the nanopore because it makes use of both the thermodynamic (pK) and kinetic (k_{on} and k_{off}) information.

Finally, the distribution of $S(0)$ over a wide range of [A] could also help determine whether there is more than one characteristic binding constant. This is important

because even if the binding sites are chemically identical, the narrow confines of a nanoscopic pore could cause the binding of analyte to one site to depend on the occupancy state of nearby sites. That is, the binding of more than one analyte of the same type to the nanopore may be either a cooperative or an anticooperative process.

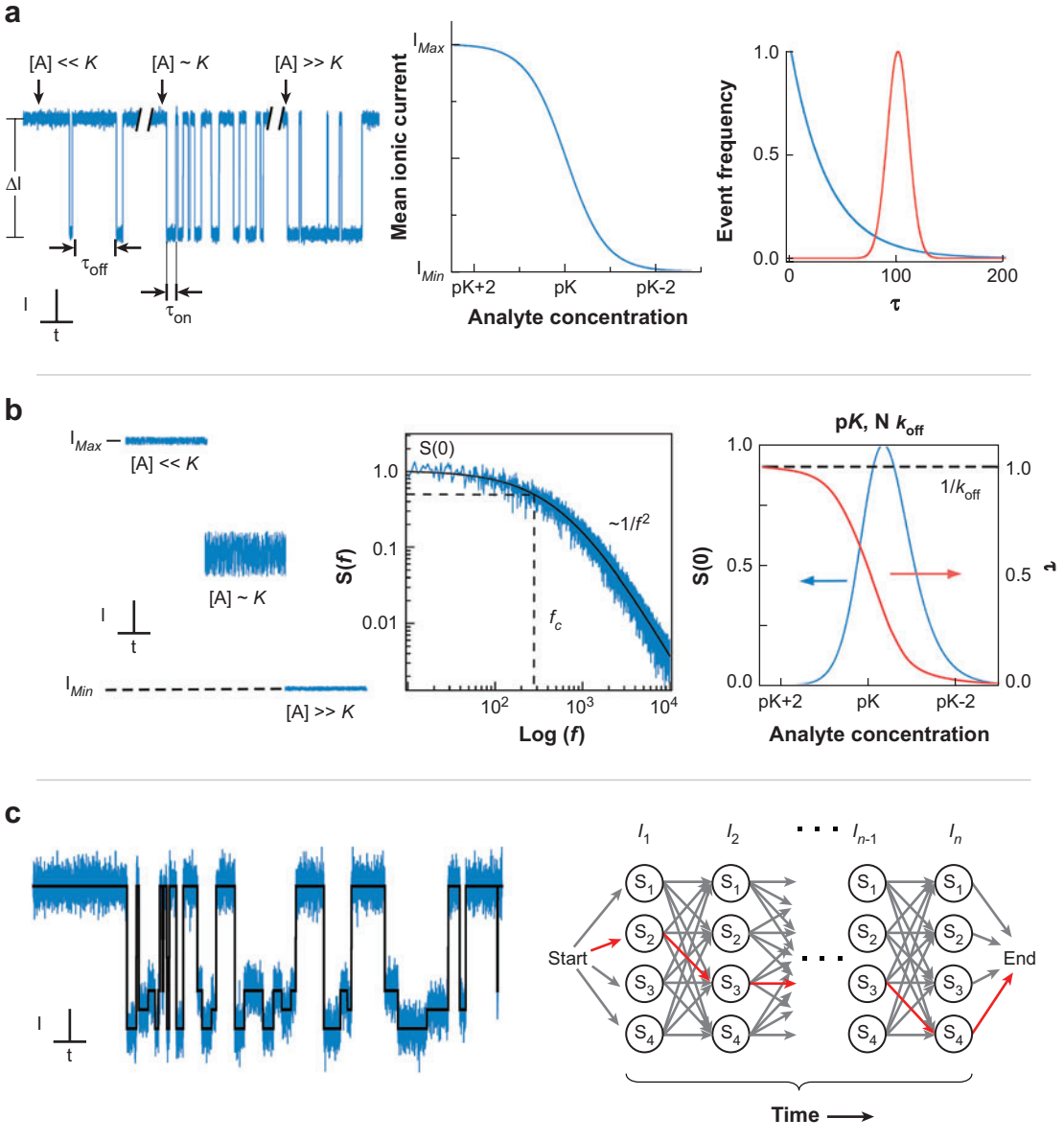

2.3. Hidden Markov Models and Viterbi Decoding Analysis

As discussed below, the interaction of polymers with a nanopore can generate ionic current time series that are much more complicated than those depicted in **Figure 2*a*** (*left*) and **2*b*** (*left*). For example, consider the noisy, multistate current recording in **Figure 2*c*** (*left*, *blue trace*). One might ask what produces the variety of conductance states and the sequence of conductance value transitions within each event.

For analytical purposes, there are two questions to be addressed. First, can persistent conductance states and patterns in the data be identified in order to reduce the events in the time series to a small number of parameters? If so, data reduction and interpretation can be greatly simplified. Second, what can be learned about the sample that caused the current blockades, given the observed data? Specifically, can the ionic current time series help determine whether the number of distinctly different types of analytes in a sample, the concentration(s) of the analyte(s), the physical or chemical information encoded in the analyte(s), and the properties of the analyte(s) change over time?

One method of analyzing this class of time series is to use the architecture of the Hidden Markov Model (HMM) (51, 52). An HMM is a statistical model of a Markov source that generates a time series of observations that are probabilistically related to the states. The observable time series is hypothesized to be made up of random variables drawn from a set of state-transition-dependent probability distributions (i.e., output distributions). In this case, a Markov source is a matrix of transition probabilities between possible states of the analyte-induced nanopore current levels. The problem is that the state of the Markov source is not directly observable (i.e., it is hidden). Instead, we can only observe a variable that is statistically related to the hidden states, namely the ionic current.

In the examples described in this review, the conductance time series is related to a particular analyte interacting with the nanopore expressed through its characteristic blockade level. The advantage of using HMM methodologies rather than more simplistic techniques becomes evident as the signals become more complex, for instance,

Figure 2

Classes of signals from nanopore-based detection and characterization of analytes. (*a*) Ionic current time series for a single nanopore in the presence of an analyte at three different concentrations (*left*); dependence of the mean current on analyte concentration (*center*); two possible lifetime distributions estimated from blockade event dwell-time analysis (*right*). (*b*) Ionic current time series with indistinct current fluctuations caused by an analyte (*left*); power spectral density of the current fluctuations (*center*); dependence of the kinetic, thermodynamic, and structural parameters derived from spectral density analysis (*right*). (*c*) Characterizing complex current time series with Hidden Markov Model (HMM)–Gaussian Mixture Model statistical analysis. *Left*: Time series data (*blue*) with a corresponding decoded state sequence (*black*). *Right*: Viterbi graph search algorithm that finds the most probable state sequence given the HMM and the data. The values of $I_1, \ldots, I_n$ represent the conductance time series from the pore that is interrogated by analyte(s), and the nodes labeled $S_1, \ldots, S_4$ represent the states in the conductance distribution. The gray arrows represent the probabilities for making transitions from one state to another in one time step. The red arrows represent one solution for a given HMM and data set.

current blockades that are characterized by steps through multiple conductance states or events that are heavily buried in noise and cannot be delineated by simple threshold methods.

The hypothetical data in **Figure 2*c*** (*left*, *blue trace*) illustrate analyte-induced ionic current blockades with overlapping states. The use of thresholding mechanisms to describe the system (i.e., assigning representative conductance values for the time series based on whether the conductance has changed by an arbitrary number of standard deviations from arbitrary mean values) results in many physically unrealistic state changes (*not shown*). In contrast, the HMM method determines the state transition probability matrix and incorporates it into a state-decoding algorithm (53), resulting in a superior description of the data set in **Figure 2*c*** (*left*, *black trace*). The Viterbi decoding algorithm is particularly useful because it makes decisions based on the whole sequence of data and is not overly influenced by outlier events in the time series or by a degree of overlap in the output distributions.

The classical Baum-Welsh training procedure, often used for HMM decoding, requires supervised training, i.e., human-labeled training sets, to optimize the parameters of the HMM. Furthermore, it requires the assumption that the noise of the system is white and independent of the blockade level, conditions that are not necessarily met for nanopore-based conductance measurements. Various research groups have proposed variations on the Baum-Welsh training procedure or have eliminated it altogether (54). These variations allow more accurate parameter estimation in the presence of correlated input data (i.e., state value plus noise) (55, 56). These methods were extensively developed for other time-correlated fields such as speech pattern recognition (57, 58) as well as for other complex time-series problems, such as economic forecasting (59).

Figure 2*c* (*right*) illustrates an HMM graph of a first-order Markov model. In this type of model, a particular state depends only on the immediate prior states, and this assumption is reasonable for reversible chemical reactions. One solution of the HMM is shown by the pathway defined by the red arrows in the graph. In the GMM-based HMM, the best state sequence of the HMM given the data is estimated by a Maximum A Posteriori (MAP) estimation procedure (60).

3. DETECTION AND CHARACTERIZATION OF NUCLEIC ACIDS WITH SINGLE NANOPORES

Figure 1*a* shows only three of the many protein ion channels found in nature. One of these, the *Staphylococcus aureus* α-hemolysin ion channel, has become an excellent model system for analytical applications for two reasons. First, unlike many channels, studies have shown that this nanopore can remain fully open for periods of up to several hours because its voltage-dependent gating behavior (i.e., the spontaneous switching between different conductance states) can be completely suppressed (11, 54). Therefore, any conductance fluctuations observed in the presence of analyte can be attributed to that agent and not to the pore itself. Second, some polymers can reside ∼500-fold longer inside this pore (∼100 μs) than would be expected from a simple one-dimensional diffusion calculation (24). The latter result is significant in that it

would otherwise be impossible to directly observe polymer-induced ionic current blockades. Specifically, without such analyte-binding interactions, there would be a statistically insignificant number of ions (~100 or fewer) that would flow past the molecule while it is inside the nanopore.

A nanopore that does not gate and that interacts with analytes that enter it is ideally suited to the task of interrogating polymers (24). For example, the α-hemolysin nanopore can also be used to detect and characterize single-stranded RNA and DNA polynucleotides. **Figure 3*a*** illustrates ionic current blockades caused by individual poly[U] RNA molecules that were added to the aqueous phase, bathing one side of the nanopore. The polymers were driven into the pore by an applied electric field (14, 16). The blockades were well defined in both amplitude and lifetime. For a poly[U] sample that was relatively monodisperse in length, the distribution of blockade lifetimes (**Figure 3*b***, *inset*) was described well by a three-component Gaussian Mixture Model (GMM). Similar experiments performed with different monodisperse lengths of poly[U] demonstrated that the two longest characteristic lifetimes were proportional to the number of bases in the polymer (**Figure 3*b***) (14). Because the contour lengths of these polymers were >52 nm, and the α-hemolysin channel had to be at least as long as a lipid bilayer is wide (~4 nm), it was assumed that the polymers were threading completely through the α-hemolysin channel.

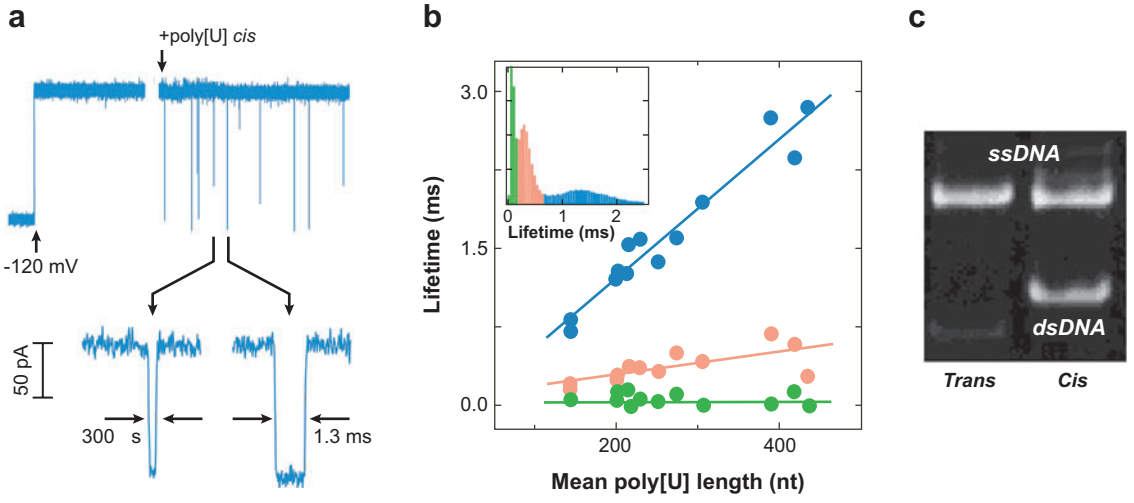

Figure 3

Detection and characterization of single-stranded polynucleotides using a single protein nanopore. (*a*) Transient ionic current blockades caused by single-stranded RNA of one length. (*b*) Residence times for different-length RNAs in the nanopore. The colors correspond to the three mean residence times estimated from blockade-event lifetime histograms for each length poly[U]. *Inset*: Residence-time histogram for 210-nucleotide-long poly[U]. (*c*) Polymerase chain reaction demonstrates that single-stranded DNA (ssDNA), but not double-stranded DNA (dsDNA), is transported through the α-hemolysin channel from the *cis* to the *trans* side. Adapted from Reference 14 with permission.

Similar results were obtained with homopolymers of single-stranded DNA (ssDNA). However, in this case the conductance blockade lifetime distributions were described by only two Gaussians. The lifetime of the longer-lived events was again proportional to the polynucleotide length. Blunt-ended double-stranded DNA (dsDNA) only caused short-lived blockades and were assumed not to thread through the pore, as single-stranded RNA and DNA polynucleotides were thought to do. More compelling evidence for this interpretation was obtained using the polymerase chain reaction (PCR) technique (**Figure 3*c***). By adding both ssDNA and dsDNA to the solution bathing one side of the nanopore, PCR was used to verify that ssDNA but not dsDNA was transported through the α-hemolysin channel (14). These results are consistent with the diameter of the α-hemolysin pore estimated from the channel's crystal structure (61), which was unknown at the time of the DNA transport measurements. dsDNA has been shown to thread through larger ion channels in a similar manner (62, 63).

If poly[U] RNA threads completely through the pore, why should there be three characteristic lifetimes for each polymer length? The events with the shortest lifetimes, which are independent of the polynucleotide length, are most likely caused by polymers entering and leaving the same pore entrance. It had been suggested that the two different longer lifetimes, which are proportional to the polymer contour length, might be due to different rates of transport for poly[U] molecules that enter the nanopore via either their 3′- or 5′-ends (14). More recent experiments and molecular dynamics simulations demonstrated that this is indeed the case (18).

4. SEQUENCING DNA WITH SINGLE NANOPORES

Because single-stranded polynucleotides can thread through a single α-hemolysin channel at ∼2 μs/base (**Figure 3*b***) essentially as straight rods, it was suggested that a single nanopore might prove useful for rapidly sequencing DNA if each of the four bases in a polynucleotide decrease the nanopore conductance by an amount that correlates with base type (i.e., A, T, G, and C for DNA). In the simplest possible scheme, the sequence would be read directly from the ionic current time series (14). If that were possible, then it would take only ∼2 ms to sequence a kilobase-long piece of DNA and only ∼6000 s to sequence an entire human genome! However, the limitations of that scheme have been noted (14). These constraints include the low signal-to-noise ratio (e.g., only ∼500 ions flow past any one base inside a nanopore) and that the rate of polymer transport through the nanopore is probably not uniform.

Recently, homopolymers containing cytosine or adenosine were shown to cause distinctly different blockade patterns in the single α-hemolysin channel current (15). Specifically, poly[C]-induced current blockades were greater in magnitude and shorter in duration than those caused by poly[A]. Moreover, a diblock copolymer of poly[C]:poly[A] caused predominantly two-step blockades that were characteristic of the poly[C] signature followed by that of the poly[A] segment (15). Some researchers suggested that this represented evidence for sequencing individual bases of DNA with a single nanopore. However, it is possible that different solution structures of

poly[C] and poly[A] (64) are responsible for the varying degrees of current blockade and residence times for the polymers driven through the nanopore.

Other schemes for sequencing DNA with nanopores were subsequently proposed. According to these hypotheses, the DNA sequence could be determined from either the transverse tunneling current flowing through a single base and two electrodes at opposite sides of a pore entrance (**Figure 4**, center) (65), the change in the voltage resulting from a single base moving across a dielectric barrier (**Figure 4**, right) (66), or the flow of current through a single-electron transistor (67). Further details on each of these DNA sequencing schemes can be found in a recent review (68).

The reliability of nanopore-based DNA sequencing using conductance measurements is limited in part by the low signal-to-noise ratio caused by too few ions flowing past each base in the pore. Conceivably, averaging the signal by using an oscillating electric field to repeatedly floss the ssDNA molecule back and forth through the pore may provide a solution to this problem (17, 69, 70). Oscillating electric fields have also been suggested to provide a means for precisely controlling the position of ssDNA

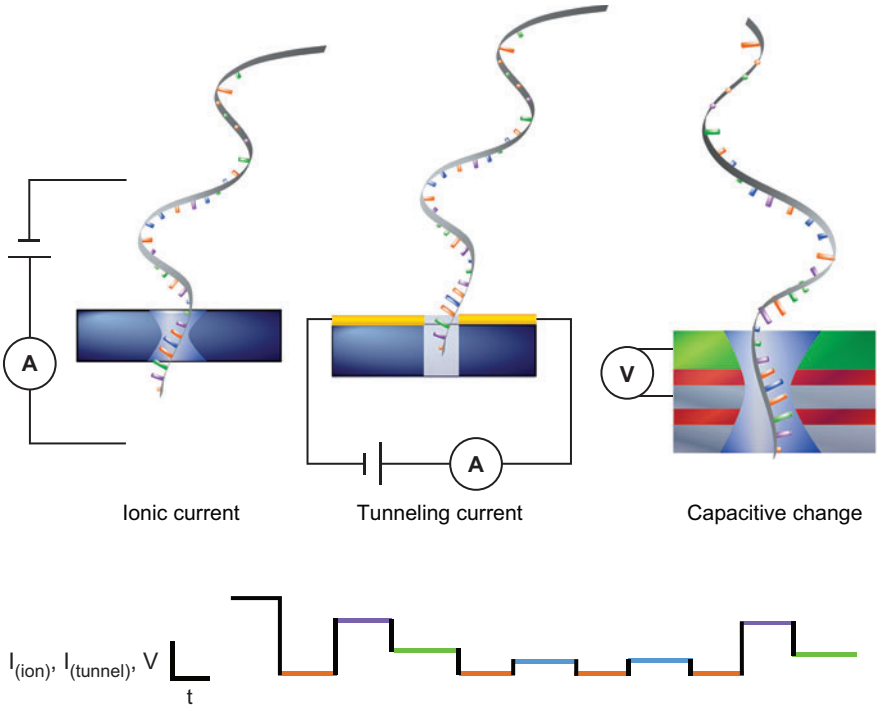

Figure 4

Proposed nanopore-based DNA sequencing schemes. *Top*, *from left to right*: direct DNA sequence readout via measurements of ionic current (14), tunneling current (65), and voltage differences (107). *Bottom*: highly simplified cartoon illustration of how each of the four different bases of DNA might produce characteristic time series recordings in each of the above schemes.

within a nanoconstriction (71). These methodologies have not yet been reduced to practice.

5. ANALYTE-INDUCED SIGNAL COMPLEXITY: FRIEND OR FOE?

Figure 5*a* illustrates conductance blockades caused by identical-length homopolymers of single-stranded poly[T], poly[C], and poly[A] as they are driven into a single α-hemolysin nanopore (17). The three polymer types can be distinguished easily from one another by visual inspection of their respective signals. Like poly[U]-induced blockades (**Figure 3*a***), the amplitude distributions for events caused by poly[C] and poly[A] can be described by single Gaussians. In contrast, the blockade distributions and patterns caused by poly[T] are much more complex. Also, the signal patterns for poly[T] depend on the direction in which the polymer is driven through the nanopore (**Figure 5*b***).

An HMM analysis (see Section 2.3, above) demonstrated that poly[T]-induced blockades, with event lifetimes as long as 2 s, were described by a GMM with ∼38 components for a polymer driven through the pore in one direction and ∼18 components when it was transported in the opposite direction (54). There is some solace in the ansatz that the complex blockade signatures are most likely related to the structure of the α-hemolysin nanopore interior (54). However, the question remains whether this degree of signal complexity is cause for celebration or grief.

Figure 5*c* illustrates a series of poly[T]-induced current blockade amplitude histograms over a wide range of blockade lifetime intervals. When presented in this manner, the relatively large number of Gaussian components needed to describe the data does not appear to be so daunting. Rather, the data take on the appearance of a spectral fingerprint (60).

It is possible that the complexity of a polymer's signals (e.g., the distribution of blockade amplitudes, as shown in **Figure 5*c***) and the HMM matrix that describes the probabilities of making a transition between a given conductance state and each of the many others may provide the means of identifying, with a high degree of certainty, a particular analyte type (60). If this is indeed the case, then it may become possible to determine how cells "think" in real time by observing changes in the cytoplasmic mRNA content in response to different stimuli (72). Of course, the nanopore would first have to be calibrated or trained with the kinds of mRNA that are thought to be produced by the cell in question.

6. ANALYTE DETECTION AND QUANTITATION USING MOLECULAR ADAPTERS

The sensor functionality of single protein nanopores can be altered with genetic engineering. For example, the native α-hemolysin channel can be rendered relatively insensitive to heavy metal divalent cations (12, 13, 73). By placing novel amino acid side chains at one entrance to the nanopore, the channel is sensitized to relatively low concentrations of divalent cations. However, this method limits the range of analytes that

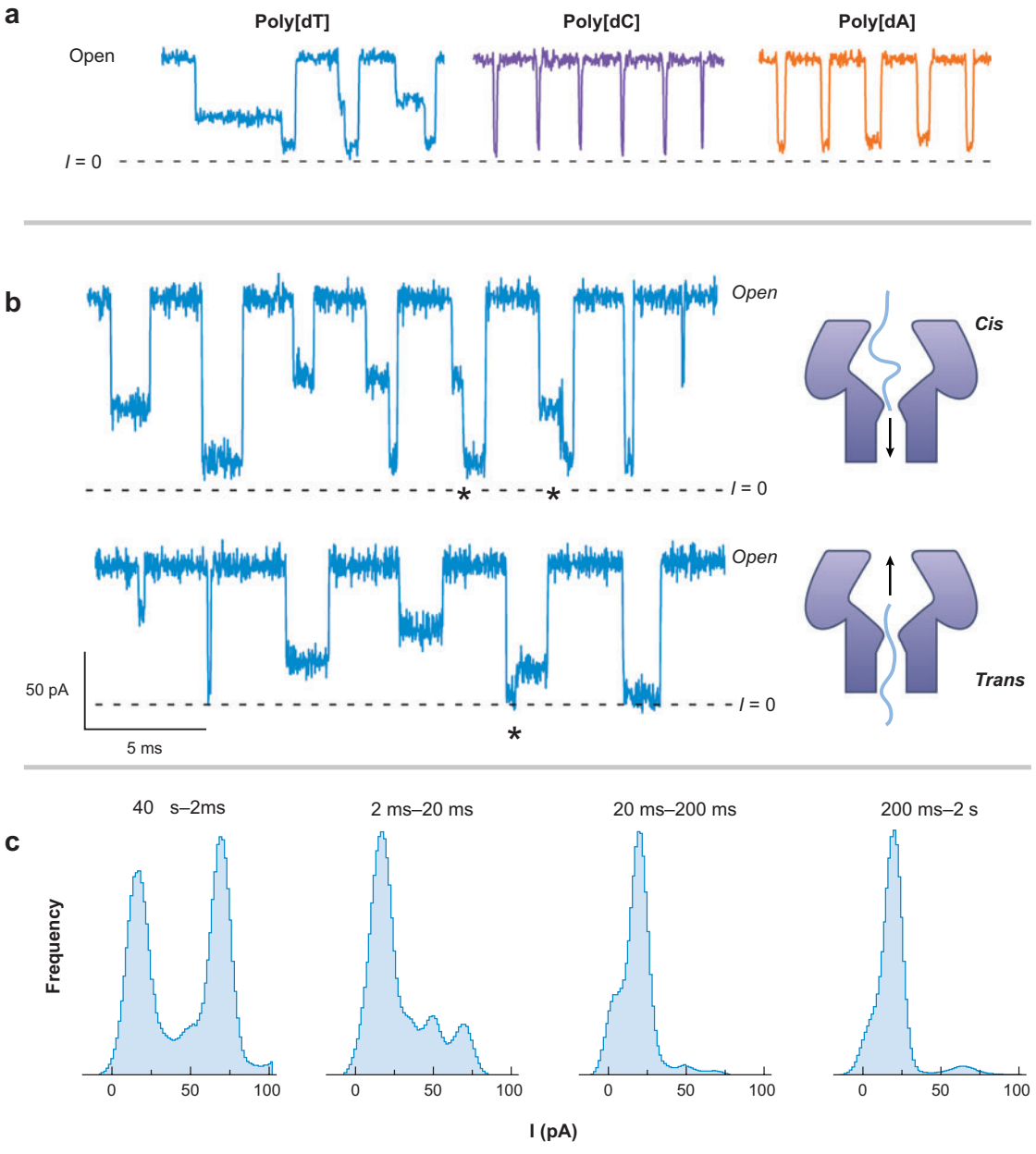

Figure 5

Complex signals caused by polynucleotides driven into a single protein nanopore. (*a*) Ionic current blockades caused by identical-length single-stranded DNA homopolymers of poly[dT], poly[dC], and poly[dA]. (*b*) Poly[dT] current blockade patterns depend on the direction in which the polynucleotide enters the pore. Note the reverse patterns for blockades are denoted by (*). (*c*) Conductance-state histograms for poly[dT] in the nanopore over a range of residence times. Adapted from References 16 and 17 with permission.

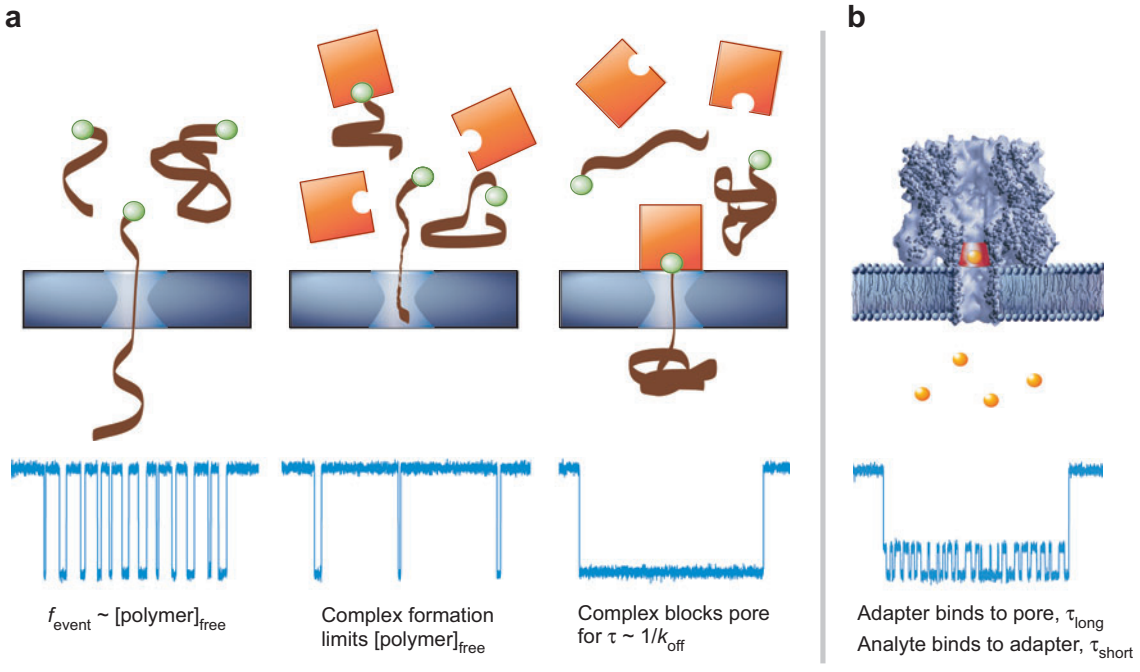

Figure 6

Detection schemes with analyte binding sites on pore-permeant macromolecules. The binding site (*green sphere*) is attached to either (*a*) a polymer whose ability to enter (or transport through) the pore depends on the presence of analyte (*orange*), or (*b*) a molecular adapter that binds to both the pore interior and an analyte of choice. Adapted from References 17 and 20 with permission.

can be detected and quantitated with a nanopore, and it is difficult to rationally design stereospecific analyte binding sites located at the pore entrance or inside the pore (13).

One way to avoid these issues is to position the analyte binding site on something other than the nanopore. Two approaches to this solution are illustrated in **Figure 6**. In one method, the binding site is placed on a polymer (**Figure 6*a***). In the absence of analyte, the polymer is driven into and through the nanopore (14), and the frequency of blockades increases with the concentration of free polymer in solution (16, 17). The presence of analyte changes the manner in which the polymer interacts with the nanopore. If the polymer is sufficiently short, the analyte inhibits the entry of polymer into the pore, decreasing the number of polymer-induced blockades per unit time in a stoichiometric fashion. Thus, the reduction in time-averaged blockade frequency is directly related to the analyte concentration (17). If the polymer is long enough to enter the pore even when bound with analyte, then the mean time that the complex is bound can be determined from the distribution of polymer–analyte-induced current blockades (17). Because different polymers give rise to different classes of nanopore current blockades, this method can be used for the simultaneous detection of multiple analytes.

The binding site can also be located within cyclic molecules (e.g., β-cyclodextrins) that can react with several types of small molecules (20). In such a case the cyclic molecule, which by chance binds to the pore interior (see Reference 24), acts as a molecular adapter. When the adapter binds to the nanopore, the conductance decreases. The subsequent binding of analytes to the adapter, when it is inside the pore, further modulates the nanopore ionic current blockade (**Figure 6*b***).

The use of polymers or molecular adapters that bind analytes confers an additional advantage over positioning the binding site on the nanopore itself: The analyte to be detected can be changed merely by replacing the polymer or adapter in solution (17).

7. SINGLE-MOLECULE FORCE SPECTROSCOPY VIA SINGLE NANOPORES

Placing a large macromolecule on one end of a polynucleotide inhibits (16, 17) or retards (17) the translocation of a polynucleotide through the nanopore (illustrated schematically in **Figure 6*a***, *right*). It has been shown that if a polymer-macromolecule complex is driven into the pore with a relatively high magnitude of the applied potential and if the voltage difference is subsequently decreased, the polymer can take a surprisingly long time (i.e., many seconds) to back-diffuse out of the nanopore (16). This finding suggested a new method to probe the interactions between the polymer and the nanopore and/or intrapolymer interactions (**Figure 7**). In fact, single nanopores provide a possible improvement for single-molecule force spectroscopy (18), because they can be used to perform many more experiments per unit time than can be done with the test molecule tethered to a solid support. In general, the ability of a molecule to enter and/or translocate through a single nanopore can be modulated by a suite of forces (e.g., electrical, chemical, optical tweezer). By modulating any of these forces, the residence time of a polymer in the pore can be altered.

A simplified version of this method (17) was used to estimate the strength of DNA hairpins using single α-hemolysin nanopores (19). The free end of the polymer could enter the pore. However, the hairpin, which is a dynamic entity, did not immediately follow the free end past the α-hemolysin channel vestibule. This study demonstrated that the lifetime of the DNA hairpin correlated with the free energy of the hairpin formation and was substantially altered by a single base mismatch. A variation on this experiment was used to estimate the time it takes to unzip duplex DNA that has an ssDNA overhang (74).

Figure 7*a* illustrates how the forces of an applied potential and an optical tweezer acting on a DNA molecule–polystyrene bead complex can be balanced when the DNA is inside the nanopore (75).This technique should eventually prove useful for controlling the rate at which individual polymers thread through a single nanopore. In addition, the ability to measure the force on the polymer inside the pore (using optical tweezers) provides another analytical tool to probe inter- and intramolecular interactions.

Figure 7*b* illustrates how nanopore-based force spectroscopy can be used to study the interactions between DNA binding proteins and polynucleotides. Once the DNA end of the DNA-protein complex is inside the pore, the applied potential is rapidly

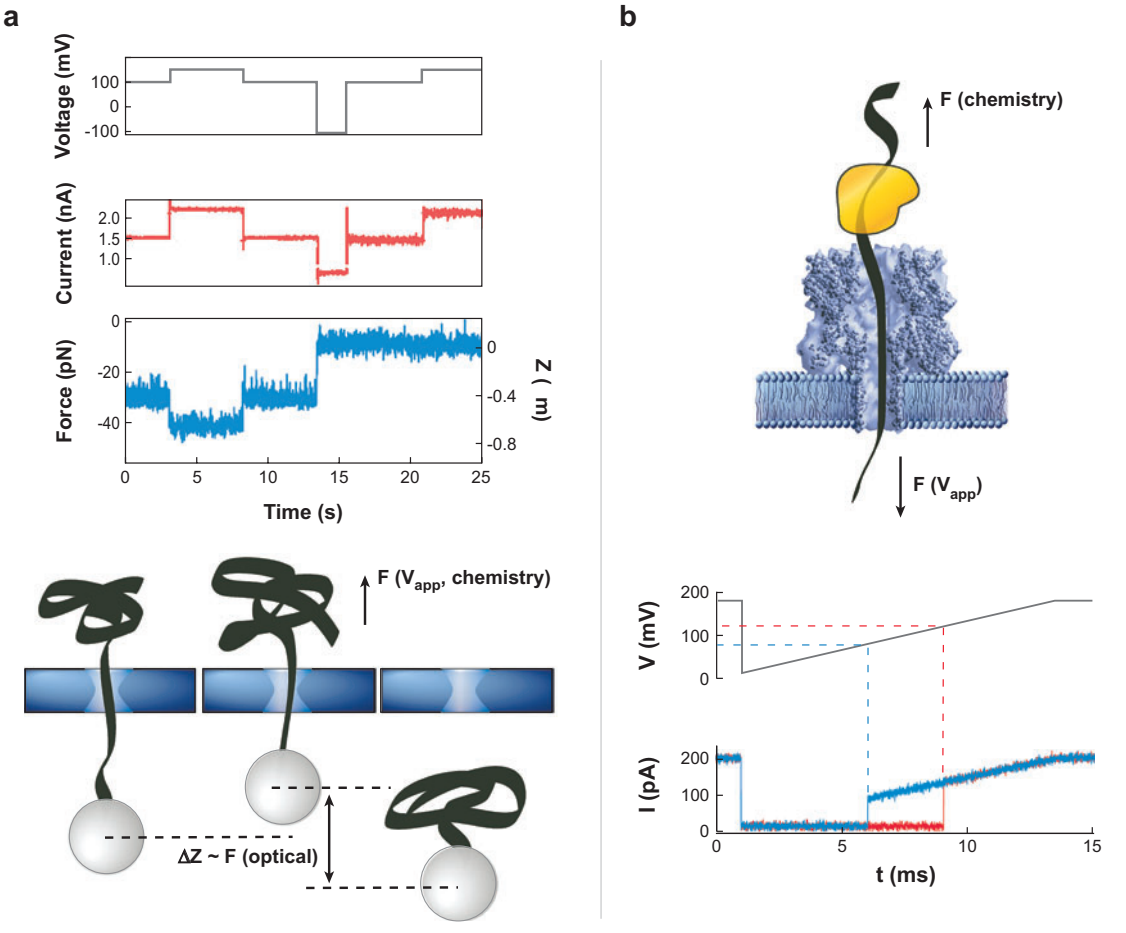

Figure 7

Two nanopore-based single-molecule force spectroscopy techniques. (*a*) The ability to apply forces (e.g., via a transmembrane electrical potential difference or an optical tweezer) to a polymer in the nanopore will enable quantitative analysis of intramolecular interactions within the polymer and of intermolecular interactions between a polymer and other molecules. (*b*) Force spectroscopy on DNA-protein complexes. *Top:* DNA-binding protein-mediated force delays the voltage driven transport of the polynucleotide through the nanopore. *Center*: Time-dependent voltage applied to an individual protein-DNA complex. *Bottom*: Single channel current from two independent voltage ramp experiments. Dissociation of the complex causes the abrupt increase in the current (*dashed lines*) to the open pore conductance. Adapted from References 16, 75, and 76 with permission.

decreased and then slowly increased. The time it takes the complex to dissociate, which leads to the complete transport of the polynucleotide through the nanopore (see, e.g., Reference 17) (**Figure 6*a***), is determined (76).

Similar experiments (77) were performed to determine the rate at which polynucleotides unzip as a function of the applied potential force loading rate. Researchers

have suggested that this approach may prove useful in estimating DNA sequences by measuring the time it takes to unzip complementary versus noncomplementary DNA strands (78).

8. DETECTION AND CHARACTERIZATION OF PROTEINS AND ANTIBODIES

Single nanopores have also been used to detect proteins and determine whether they are in a native or unfolded state. For example, by placing a binding site for a protein or antibody on one end of a polynucleotide (**Figure 6*a***), investigators showed that a single nanopore can be used to detect protein and antibodies with a protein ion channel that normally has no affinity for either analyte (17). In contrast, single α-hemolysin channels were used to directly detect short, charged polypeptides that have no known physiological relationship to the nanopore (79, 80).

It is also possible to detect full-length proteins with high specificity by using ion channels that normally interact with them. *Bacillus anthracis*, the bacteria that causes anthrax-related cell death, secretes three toxins: protective antigen (PA83, ~83 kg/mol), lethal factor (LF, ~89 kg/mol), and edema factor (EF, ~90 kg/mol). *In vivo*, PA83 binds to cells and is cleaved into two fragments. The 63-kg/mol fragment, PA63, remains associated with cell membranes and forms a transmembrane ion channel. Either LF or EF binds to the PA63 channel (**Figure 1*a***) to form lethal or edema toxins, respectively; these complexes are subsequently endocytosed. The pH of the endosome is decreased and LF or EF is transported into the cytosol, causing cell death (81). The binding of either LF or EF to a PA63 ion channel in planar bilayer membranes converts the nanopore's current-voltage relationship from slightly nonlinear to strongly rectifying. This effect was graded with either the LF or the EF concentration, and the apparent binding constants were ~50 pM (30). Also, an antibody against PA63, which has no effect on the nanopore's *I-V* relationship, completely inhibits the ability of LF to alter the nanopore's conductance at any voltage (30). Thus, the anthrax PA63 ion channel can be used as a sensitive detector for LF or EF and as a high-throughput screening device for potential therapeutic agents against anthrax infection.

In addition to detecting protein fragments and full-length proteins, single nanopores can be used to determine whether individual soluble proteins are in their folded (native) conformation, or completely unfolded. This task is usually addressed using circular dichroism on an ensemble of the protein. As is illustrated in **Figure 8*a***, in the absence of guanidinium chloride [Gdm-HCl], the single α-hemolysin channel current was quiescent, even in the presence of a maltose binding protein from *E. coli*. The latter protein, which contains no stabilizing disulfide bonds, comprises 370 amino acid side chains (~40 kg/mol molecular mass) and is negatively charged at physiological pH. Interestingly, for concentrations of Gdm-HCl greater than 0.8 M, the protein caused well-defined current blockades (82). Control experiments demonstrated that 0.8 M of Gdm-HCl denatures the maltose binding protein but does not significantly affect the α-hemolysin channel conductance. Thus, the denatured protein appears to be driven into the α-hemolysin nanopore

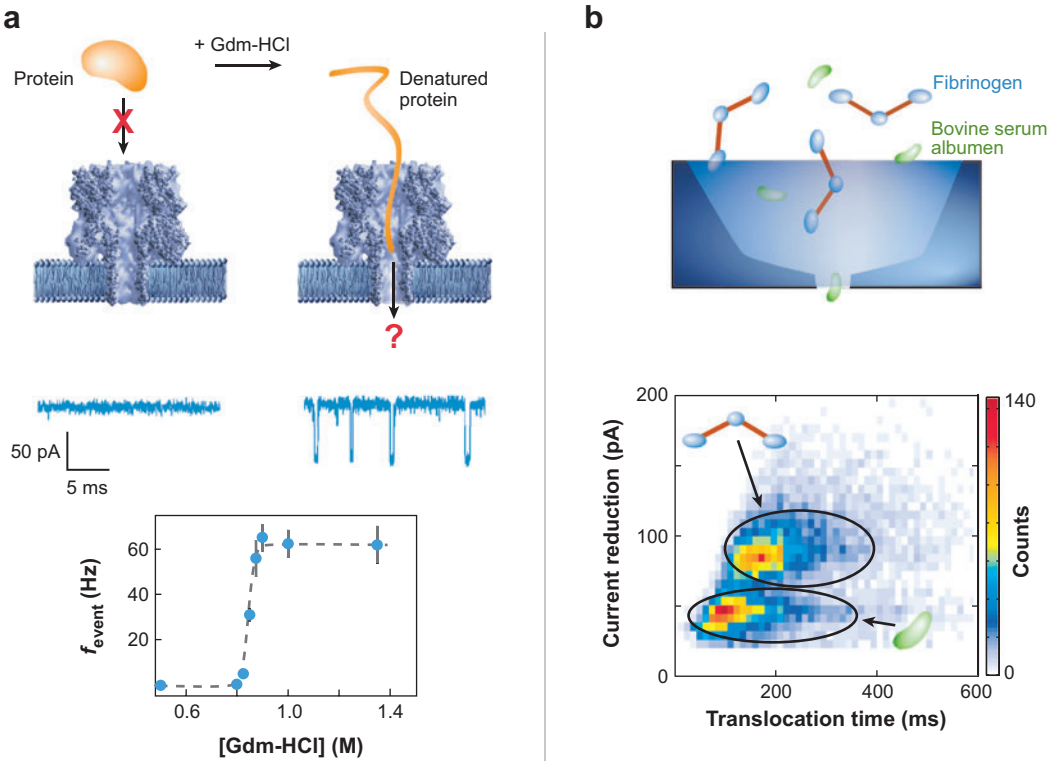

Figure 8

Direct detection of proteins with single nanopores. (*a*) A protein in its native conformation is too large to enter a single α-hemolysin nanopore (*top left*). Addition of guanidinium chloride greater than 0.8 M denatures the protein. The denatured protein can then enter the nanopore and cause transient current blockades (*top right*, *middle*). The frequency of blockades increases with increasing denaturation concentration (*bottom*). (*b*) The ability of two different proteins (fibrinogen and bovine serum albumin) to partition into a solid-state nanopore was determined from single channel recordings. The results are plotted in terms of the mean current blockade amplitudes versus the residence times of the proteins in the nanopore. Adapted from References 82 and 86 with permission.

in a manner similar to polynucleotides (14, 16, 84) and dextran sulfate molecules (83).

Solid-state nanopores have also proven to be effective for detecting proteins. A single solid-state elliptical nanopore with an orifice ~58 nm by 50 nm and 20 nm thick was used to detect bovine serum albumin (BSA) at low concentration (85). Smaller single solid-state nanopores (~16 nm in diameter, ~10 nm long) were used to detect two different proteins: BSA (~66 kg/mol) and fibrinogen (340 kg/mol) (86). Distinctly different patterns in a plot of the protein-induced current blockade amplitude versus the protein residence times in the pore (**Figure 8*b***) were observed for fibrinogen and BSA, and thereby suggest that the nanopore was able to discriminate

between the two proteins. Based on the influence of BSA on the pore conductance as a function of pH, the charge on that protein was estimated for each pH value. The transport of the protein through the nanopore, as judged by conductance measurements, was confirmed using chemiluminescence with fluorescently labeled versions of the polypeptide.

9. SINGLE-MOLECULE MASS SPECTROMETRY USING A NANOPORE

Nonelectrolyte polymers have been used to estimate the size of ion channels by comparing the relative conductivity of an ion channel with the addition of polymers having a range of molecular weights or sizes (22, 24, 26, 27). By approaching the problem from the reverse (i.e. probing the size of the polymer molecules with a nanopore of known geometry), then a single nanopore can provide the basis for accurate measurements for the sizes of individual molecules in solution.

The principle of sizing nanopores with polymers is simple. Some polymers (e.g., PEG) decrease the bulk electrolyte conductivity and those molecules that are small enough to enter the pore will decrease the single-channel conductance. The size of the pore is then estimated by determining the largest polymer that can enter the pore and knowing the hydrodynamic radii of the polymers.

In principle, the polymer-induced decrease in pore conductance should scale with the size of the polymer in the pore: Larger polymers should decrease the conductance more than smaller ones. The question, then, is how small of a difference between the polymer molecular masses can one determine using a nanopore.

A representation of the experiment is illustrated in **Figure 9*a***. PEG added to the solution bathing one side of the membrane caused well-defined polymer-induced fluctuations in the ionic current (**Figure 9*b***). The average residence time of the polymers in the pore was on the order of 1 ms (24, 28). Representative data for polydisperse ($MW_{avg} = 1500$ g/mol) and monodisperse ($MW = 1294$ g/mol) PEG were collected until a large number ($>10^5$) of individual polymer-pore interactions were observed to ensure a statistically significant sampling of the data (29). There were clearly discernible differences in the depths of the current blockades caused by the polydisperse PEG sample, whereas the monodisperse PEG caused blockades that were virtually all of the same mean conductance value. An all-points histogram of the entire current time series does not permit accurate decoding of the blockades caused by each of the differently sized PEGs in the dispersion (*not shown*).

To resolve the individual components within the mixture, each blockade event is represented by its mean current value. A histogram made from the mean current blockade amplitudes clearly resolves ~24 PEG n-mers ranging from $n = 25$ to $n = 49$ ($HO(CH_2CH_2O)_nH$) (**Figure 9*c***, *red*) and correlated 1:1 with a matrix-assisted laser desorption/ionization–time-of-flight mass spectrum of the sample. Calibration of the mass of the sample was achieved by an identical analysis of PEG-1294 (**Figure 9*c***, *blue*). Experimental data were reduced with an HMM/GMM Viterbi decoding analysis (**Figure 9*c***, *black*), which allowed access to the residence time for each polymer

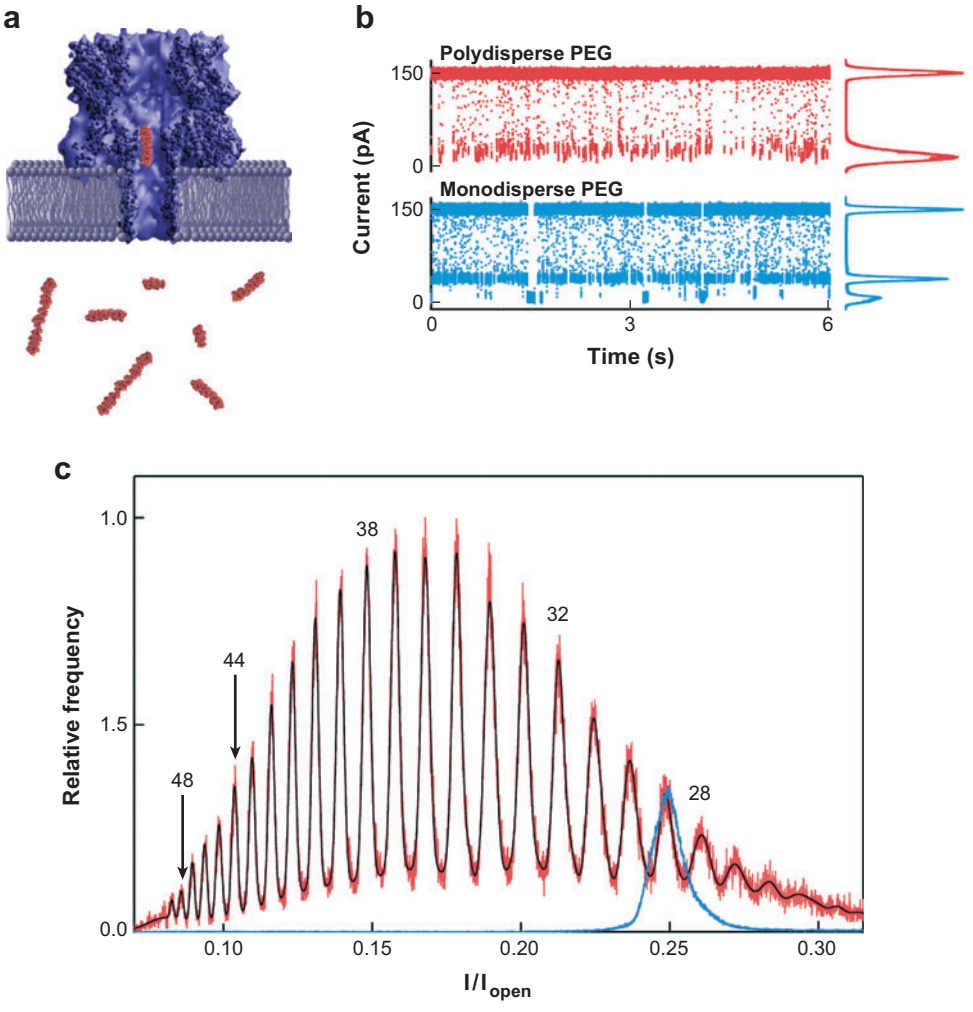

Figure 9

(*a*) Representation of single-molecule mass spectrometry of polymers using a single α-hemolysin nanopore. (*b*) The dispersion of conductance blockade amplitudes for polydisperse poly(ethylene glycol) (PEG) (*red*) is much greater than that for a monodisperse sample of the polymer (*blue*). (*c*) Conductance-based mass distributions for polydisperse (*red*) and monodisperse (*blue*) PEG. The numbers correspond to the degree of polymerization of the PEGs. Adapted from Reference 29 with permission.

in the mixture, thereby permitting two dimensions of discrimination for a single molecular component (blockade depth and time). This technique can be easily extended to any polymer analytes [such as poly(styrene sulfonate); see Reference 87] that interact with the interior of the nanopore.

10. THEORETICAL ADVANCES IN MODELING POLYMER TRANSPORT THROUGH SINGLE NANOPORES

The development of analytical theories and significant advances in theoretical chemistry and molecular simulation techniques have provided valuable insights into the mechanisms of polymer transport through nanopores. Initially, several analytical treatments describing the problem of polymer translocation through a narrow pore were undertaken. Some of those studies focused on predicting the dependence of polynucleotide residence time in a nanopore as a function of the polymer length (88, 89). Three different models (**Figure 10*b***) suggest that (*a*) the dynamics of the polymer chain in the bulk gives rise to an entropic barrier (90, 91), (*b*) the polymer chain strongly interacts with the nanopore (i.e., the theory ignores the part of the chain that is free in solution) (92), and (*c*) the motion of the flexible polymer over the free-energy barrier is treated as a one-dimensional piece or kink within the chain (the kink provides a time-dependent solution to the Kramers problem) (93–95). Interestingly, several of these theories predict that the residence time of a polymer in the pore increases in proportion to the polymer contour length in the presence of an applied electrostatic potential, as was determined experimentally (14). Clearly, there is a need for new experiments to better distinguish among these different models.

Recently, a theory describing nanopore-based single-molecule force spectroscopy experiments was developed (96) and applied to the unzipping of DNA hairpins through a single biological nanopore (97). The authors applied either a linear cubic or cusp free energy surface to the Kramers model to find an analytical expression for the rate of activation as a function of the applied force. This expression leads to the probability distribution of the rupture forces that can be compared to experimental results. A purely theoretical treatment was also used to determine the error associated with the unzipping of DNA (91, 92, 98) and the estimation of the DNA sequence (90, 99–102). The error in this approach decreases exponentially with the number of unzipping attempts (103).

In addition to the analytical developments summarized above, microscopically detailed molecular simulations of macromolecular transport through biological (104, 105) and solid-state (106–108) nanopores have provided further insight into these processes that have remained elusive when studied with analytical methods alone. The simulations enable a visualization, at the atomic level of detail, of how ions and macromolecules stochastically electrodiffuse through very small structures (**Figure 10*a***). In one study (104), the average ionic occupancy of the transmembrane pore, osmotic permeability, current-voltage relationships, and selectivity for charged ions can be estimated. These powerful computational methods are also being used to aid the rational design of complex solid-state nanopores for DNA sequencing efforts (107, 109) as well as to study the effects of single-nucleotide polymorphisms and the interactions between DNA and DNA-binding proteins (110).

In contrast to brute-force, atomistically detailed simulations, the Poisson-Nernst-Planck theory (PNP) is a simple, coarse-grained approach for modeling ion transport in single nanopores. Significant advances in the development of computational algorithms for carrying out PNP calculations in biological nanopores have occurred over

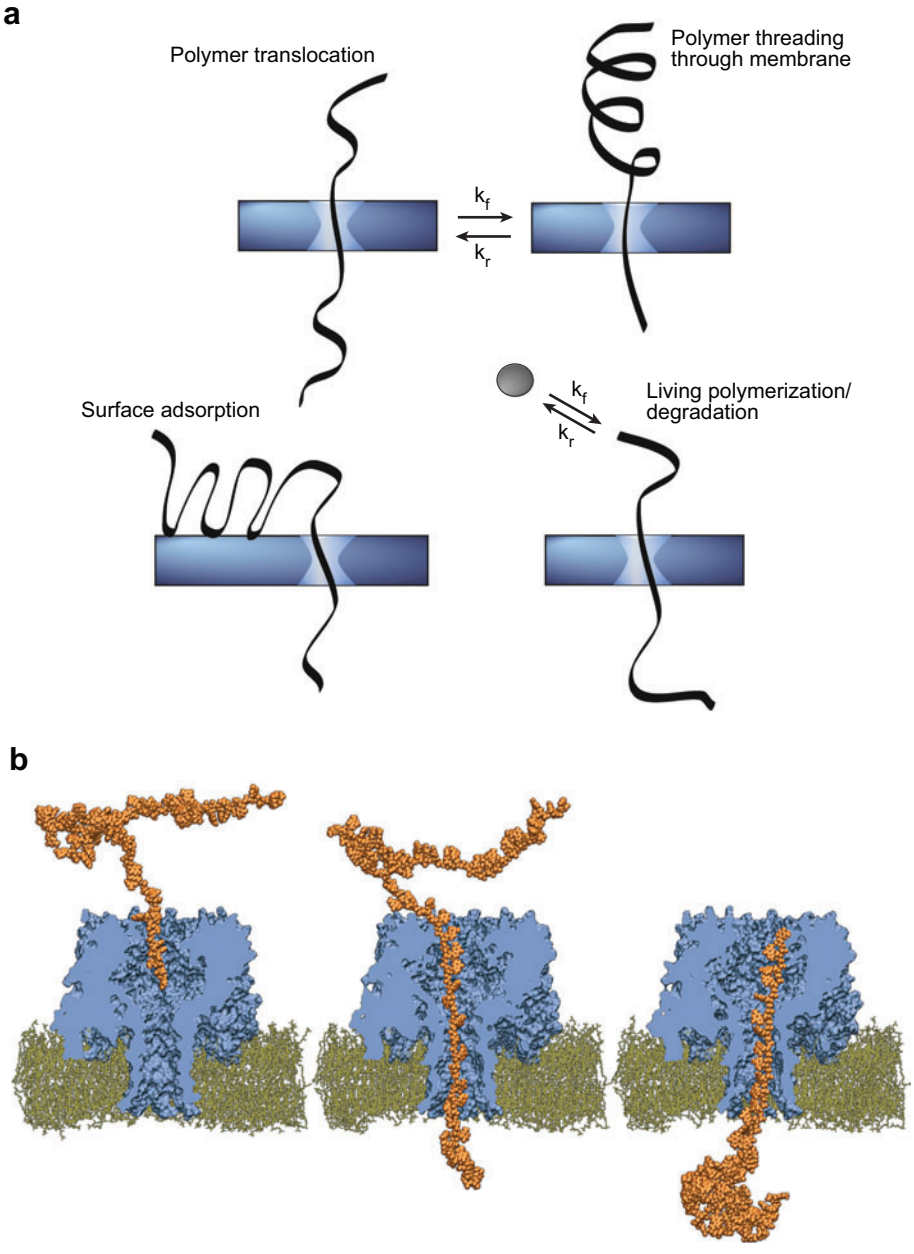

Figure 10

Theoretical methods for polymer-nanopore studies. (*a*) Analytical approaches for the study of polymer translocation through single nanopores also provide keen insight into the process. (*b*) Molecular dynamics simulation of a polynucleotide being driven through a single α-hemolysin nanopore. Courtesy of Aleksei Aksimientiev (University of Illinois at Urbana-Champaign). Adapted from References 90, 91, and 120 with permission.

the past two decades (111–115), and the theory has recently been shown to be an effective component of hybrid and multiscale modeling frameworks (105, 116, 117). These results will undoubtedly enhance our ability to understand the fundamental physics of macromolecular transport through nanopores. The properties predicted from the calculations will also aid in the design of nanopores for many analytical purposes.

11. SUMMARY

This review describes some of the experimental and theoretical efforts applied to the development of single protein and solid-state nanopores for a wide variety of applications, including the detection and quantitation of ions, proteins, polypeptides and polynucleotides; single-molecule force spectroscopy; high-throughput screening against biological warfare agents; and a conductance-based mass spectrometry that should prove to be complementary to existing mass spectrometry techniques. Single nanopores also have the potential to provide linchpin technologies useful for rapid DNA sequencing and proteomic analysis.

The nanoporous sensor community is currently divided into two camps largely based on the origin of the nanopores used. Although both biological and solid-state pores have been successfully applied to chemical analysis, biological nanopores have a ~3.8-billion-year head start on development, and have perfected precision chemical modification of the interior of the pore wall. Solid-state nanopores offer the promise of improved long-term stability, yet precise physical and chemical modification remains an elusive goal. Indeed, if the α-hemolysin protein ion channel could speak, it might be justified in quoting Mark Twain: "The reports of my death have been greatly exaggerated."

As with many other analytical techniques, the choice of nanopore will be determined by the application. It is also possible that a combination of biological and solid-state nanopores in a hybrid platform will become a formidable partnership for precision analytical measurements.

Nature demonstrates that a good strategy for the unambiguous identification of a wide range of analytes is to employ many different ion channels, each with a high degree of selectivity for a particular analyte. This approach seems likely to be true if nanopore-based sensors can be made practical in robust matrices (121).

ACKNOWLEDGMENTS

Supported in part by the Office of Law Enforcement Standards at the National Institute of Standards and Technology.

DISCLOSURE STATEMENT

The authors have filed a patent application for the technology described in Section 9 (polymer analysis using nanopores).

LITERATURE CITED

1. Coulter WH. 1953. *U.S. Patent No. 2,656,508*
2. DeBlois RW, Bean CP. 1970. Counting and sizing of submicron particles by resistive pulse technique. *Rev. Sci. Instrum.* 41:909–16
3. Ito T, Sun L, Crooks RM. 2003. Simultaneous determination of the size and surface charge of individual nanoparticles using a carbon nanotube–based Coulter counter. *Anal. Chem.* 75:2399–406
4. Saleh OA, Sohn LL. 2003. Direct detection of antibody-antigen binding using an on-chip artificial pore. *Proc. Natl. Acad. Sci. USA* 100:820–24
5. Uram JD, Ke K, Hunt AJ, Mayer M. 2006. Label-free affinity assays by rapid detection of immune complexes in submicrometer pores. *Angew. Chem. Intl. Ed.* 45:2281–85
6. Hodgkin AL, Huxley AF. 1952. Currents carried by sodium and potassium ions through the membrane of the giant axon of *Loligo*. *J. Physiol. Lond.* 116:449–72
7. Katz B. 1966. *Nerve*, *Muscle*, *Synapse*. New York: McGraw-Hill
8. Henry JP, Chich JF, Goldschmidt D, Thieffry M. 1989. Blockade of a mitochondrial cationic channel by an addressing peptide: an electrophysiological study. *J. Membr. Bio.* 112:139–47
9. Simon SM, Blobel G. 1991. A protein-conducting channel in the endoplasmic reticulum. *Cell* 65:371–80
10. Bezrukov SM, Kasianowicz JJ. 1993. Current noise reveals protonation kinetics and number of ionizable sites in an open protein ion channel. *Phys. Rev. Lett.* 70:2352–55
11. Kasianowicz JJ, Bezrukov SM. 1995. Protonation dynamics of the α-toxin ion channel from spectral analysis of pH-dependent current fluctuations. *Biophys. J.* 69:94–105
12. Braha O, Walker B, Cheley S, Kasianowicz JJ, Song LZ, et al. 1997. Designed protein pores as components for biosensors. *Chem. Biol.* 4:497–505
13. Kasianowicz JJ, Burden DL, Han LC, Cheley S, Bayley H. 1999. Genetically engineered metal ion binding sites on the outside of a channel's transmembrane β-barrel. *Biophys. J.* 76:837–45
14. Kasianowicz JJ, Brandin E, Branton D, Deamer DW. 1996. Characterization of individual polynucleotide molecules using a membrane channel. *Proc. Natl. Acad. Sci. USA* 93:13770–73
15. Akeson M, Branton D, Kasianowicz JJ, Brandin E, Deamer DW. 1999. Microsecond time-scale discrimination among polycytidylic acid, polyadenylic acid, and polyuridylic acid as homopolymers or as segments within single RNA molecules. *Biophys. J.* 77:3227–33
16. Henrickson SE, Misakian M, Robertson B, Kasianowicz JJ. 2000. Driven DNA transport into an asymmetric nanometer-scale pore. *Phys. Rev. Lett.* 85:3057–60
17. Kasianowicz JJ, Henrickson SE, Weetall HH, Robertson B. 2001. Simultaneous multianalyte detection with a nanometer-scale pore. *Anal. Chem.* 73:2268–72
18. Mathe J, Aksimentiev A, Nelson DR, Schulten K, Meller A. 2005. Orientation discrimination of single-stranded DNA inside the α-hemolysin membrane channel. *Proc. Natl. Acad. Sci. USA* 102:12377–82

19. Vercoutere W, Winters-Hilt S, Olsen H, Deamer D, Haussler D, Akeson M. 2001. Rapid discrimination among individual DNA hairpin molecules at single-nucleotide resolution using an ion channel. *Nat. Biotech.* 19:248–52
20. Gu LQ, Braha O, Conlan S, Cheley S, Bayley H. 1999. Stochastic sensing of organic analytes by a pore-forming protein containing a molecular adapter. *Nature* 398:686–90
21. Kullman L, Winterhalter M, Bezrukov SM. 2002. Transport of maltodextrins through maltoporin: a single-channel study. *Biophys. J.* 82:803–12
22. Krasilnikov OV, Sabirov RZ, Ternovsky VI, Merzliak PG, Muratkhodjaev JN. 1992. A simple method for the determination of the pore radius of ion channels in planar lipid bilayer membranes. *FEMS Microbiol. Immun.* 105:93–100
23. Bezrukov SM, Vodyanoy I, Parsegian VA. 1994. Counting polymers moving through a single-ion channel. *Nature* 370:279–81
24. Bezrukov SM, Vodyanoy I, Brutyan RA, Kasianowicz JJ. 1996. Dynamics and free energy of polymers partitioning into a nanoscale pore. *Macromolecules* 29:8517–22
25. Movileanu L, Bayley H. 2001. Partitioning of a polymer into a nanoscopic protein pore obeys a simple scaling law. *Proc. Natl. Acad. Sci. USA* 98:10137–41
26. Bezrukov SM, Kasianowicz JJ. 2002. Dynamic partitioning of neutral polymers into a single ion channel. In *Structure and Dynamics of Confined Polymers*, ed. JJ Kasianowicz, MSZ Kellermayer, DW Deamer, pp. 117–30. Dordrecht, Netherlands: Kluwer
27. Krasilnikov OV. 2002. Sizing channels with neutral polymers. In *Structure and Dynamics of Confined Polymers*, ed. JJ Kasianowicz, MSZ Kellermayer, DW Deamer, pp. 97–116. Dordrecht, Netherlands: Kluwer
28. Krasilnikov OV, Rodrigues CG, Bezrukov SM. 2006. Single polymer molecules in a protein nanopore in the limit of a strong polymer-pore attraction. *Phys. Rev. Lett.* 97:018301
29. Robertson JWF, Rodrigues CG, Stanford VM, Rubinson KA, Krasilnikov OV, Kasianowicz JJ. 2007. Single-molecule mass spectrometry in solution using a solitary nanopore. *Proc. Natl. Acad. Sci. USA* 104:8207–11
30. Halverson KM, Panchal RG, Nguyen TL, Gussio R, Little SF, et al. 2005. Anthrax biosensor: protective antigen ion channel asymmetric blockade. *J. Biol. Chem.* 280:34056–62
31. Li J, Stein D, McMullan C, Branton D, Aziz MJ, Golovchenko JA. 2001. Ion-beam sculpting at nanometre length scales. *Nature* 412:166–69
32. Li JL, Gershow M, Stein D, Brandin E, Golovchenko JA. 2003. DNA molecules and configurations in a solid-state nanopore microscope. *Nat. Mater.* 2:611–15
33. Storm AJ, Chen JH, Ling XS, Zandbergen HW, Dekker C. 2003. Fabrication of solid-state nanopores with single-nanometre precision. *Nat. Mater.* 2:537–40
34. Heng JB, Ho C, Kim T, Timp R, Aksimentiev A, et al. 2004. Sizing DNA using a nanometer-diameter pore. *Biophys. J.* 87:2905–11
35. Fologea D, Gershow M, Ledden B, McNabb DS, Golovchenko JA, Li JL. 2005. Detecting single-stranded DNA with a solid-state nanopore. *Nano Lett.* 5:1905–9

36. Kim MJ, Wanunu M, Bell DC, Meller A. 2006. Rapid fabrication of uniformly sized nanopores and nanopore arrays for parallel DNA analysis. *Adv. Mater.* 18:3149–53
37. Kim MJ, McNally B, Murata K, Meller A. 2007. Characteristics of solid-state nanometre pores fabricated using a transmission electron microscope. *Nanotechnology* 18:205302
38. Li NC, Yu SF, Harrell CC, Martin CR. 2004. Conical nanopore membranes: preparation and transport properties. *Anal. Chem.* 76:2025–30
39. Siwy Z, Dobrev D, Neumann R, Trautmann C, Voss K. 2003. Electro-responsive asymmetric nanopores in polyimide with stable ion-current signal. *Appl. Phys. A* 76:781–85
40. Horn R, Lange K. 1983. Estimating kinetic constants from single channel data. *Biophys. J.* 43:207–23
41. Chay TR, Kang HS, Chay SC. 1988. Analyzing stochastic events in multi-channel patch clamp data. *Biol. Cyber.* 58:19–33
42. Ball FG, Sansom MSP. 1989. Ion-channel gating mechanisms: model identification and parameter-estimation from single channel recordings. *Proc. Royal Soc. Lond. B* 236:385–416
43. Magleby KL, Weiss DS. 1990. Estimating kinetic parameters for single channels with simulation. *Biophys. J.* 58:1411–26
44. Colquhoun D, Hawkes AG. 1981. On the stochastic properties of single ion channels. *Proc. Royal Soc. Lond. B* 211:205–35
45. Qin F, Auerbach A, Sachs F. 1996. Estimating single-channel kinetic parameters from idealized patch-clamp data containing missed events. *Biophys. J.* 70:264–80
46. Qin F, Auerbach A, Sachs F. 1997. Maximum likelihood estimation of aggregated Markov processes. *Biophys. J.* 264:375–83
47. Stevens CF. 1972. Inferences about membrane properties from electrical noise measurements. *Biophys. J.* 12:1028–47
48. DeFelice LJ. 1981. *Introduction to Membrane Noise*. New York: Plenum
49. Machlup S. 1954. Noise in semiconductors: spectrum of a 2-parameter random signal. *J. Appl. Phys.* 25:341–43
50. Kasianowicz JJ, Henrickson SE, Misakian M, Lerman JC, Panchal RG, et al. 2007. The detection and characterization of ions, DNA, and proteins using nanometer-scale pores. In *Handbook of Biosensors and Biochips*, ed. RS Marks, DC Cullen, I Karube, CR Lowe, HH Weetall. New York: Wiley
51. Baum L. 1972. An inequality and associated maximization technique in statistical estimation of probabilistic functions of a Markov process. *Inequalities* 3:1–8
52. Redner RA, Walker HF. 1984. Mixture densities, maximum likelihood and the EM algorithm. *SIAM Rev.* 26:195–237
53. Vitterbi AJ. 1967. Error bounds for convolutional codes and an asymmetrically optimum decoding algorithm. *IEEE Trans. Inf. Theory* IT-13:260–67
54. Kasianowicz JJ, Henrickson SE, Misakian M, Weetall HH, Robertson B, Stanford V. 2002. Physics of DNA threading through a nanometer pore and applications to simultaneous multianalyte sensing. In *Structure and Dynamics of Confined Polymers*, ed. JJ Kasianowicz, MSZ Kellermayer, DW Deamer, pp. 141–64. Dordrecht, Netherlands: Kluwer

55. Qin F, Auerbach A, Sachs F. 2000. Hidden Markov modeling for single channel kinetics and correlated noise. *Biophys J.* 79:1928–44
56. Venkataramanan L, Walsh JL, Kuc R, Sigworth FJ. 1998. Identification of Hidden Markov Models for ion channel currents. Part I: Colored background noise. *IEEE Trans. Sig. Proc.* 46:1901–15
57. Rabiner LR. 1989. A tutorial on Hidden Markov Models and selected applications in speech recognition. *Proc. IEEE* 77:257–86
58. Rabiner LR, Juang BH. 1986. An introduction to Hidden Markov Models. *IEEE ASSP Mag.* 3:4–16
59. Fraser AM, Dimitriadis A. 1993. Forecasting probability densities by using Hidden Markov Models with mixed states. In *Time Series Prediction*, ed. AS Weigend, NA Gershenfeld. Santa Fe, NM: Addison-Wesley
60. Stanford VM, Kasianowicz JJ. 2004. *Transport of DNA through a single nanometer-scale pore: evolution of signal structure*. Presented at IEEE Workshop Genomic Signal Process. Stat., Baltimore, MD
61. Song LZ, Hobaugh MR, Shustak C, Cheley S, Bayley H, Gouaux JE. 1996. Structure of staphylococcal α-hemolysin, a heptameric transmembrane pore. *Science* 274:1859–66
62. Szabo I, Bathori G, Tombola F, Brini M, Coppola A, Zoratti M. 1997. DNA translocation across planar bilayers containing *Bacillus subtilis* ion channels. *J. Biol. Chem.* 272:25275–82
63. Szabo I, Bathori G, Tombola F, Coppola A, Schmehl I, et al. 1998. Double-stranded DNA can be translocated across a planar membrane containing purified mitochondrial porin. *FASEB J.* 12:495–502
64. Saenger W. 1984. *Principles of Nucleic Acid Structure*. New York: Springer-Verlag
65. Zwolak M, Di Ventra M. 2005. Electronic signature of DNA nucleotides via transverse transport. *Nano Lett.* 5:421–24
66. Gracheva ME, Aksimentiev A, Leburton JP. 2006. Electrical signatures of single-stranded DNA with single base mutations in a nanopore capacitor. *Nanotechnology* 17:3160–65
67. Mali P, Lal RK. 2004. The dnaSET: A novel device for single-molecule DNA sequencing. *IEEE Trans. Electron Dev.* 51:2004–12
68. Zwolak M, Di Ventra M. 2007. Physical approaches to DNA sequencing and detection. *Rev. Mod. Phys.* 80:141–65
69. Kasianowicz JJ. 2004. Nanopores. Flossing with DNA. *Nature Materials* 3:355–65
70. Sigalov G, Comer J, Timp G, Aksimentiev A. 2008. Detection of DNA sequences using an alternating electric field in a nanopore capacitor. *Nano Lett.* In press
71. Polonsky S, Rossnagel S, Stolovitzky G. 2007. Nanopore in metal-dielectric sandwich for DNA position control. *Appl. Phys. Lett.* 91:153103
72. Kasianowicz JJ. 2002. Nanometer-scale pores: potential applications for analyte detection and DNA characterization. *Dis. Markers* 18:185–91
73. Menestrina G, Mackman N, Holland IB, Bhakdi S. 1987. *Escherichia coli* hemolysin forms voltage-dependent ion channels in lipid membranes. *Biochim. Biophys. Acta* 905:109–17

74. Sauer-Budge AF, Nyamwanda JA, Lubensky DK, Branton D. 2003. Unzipping kinetics of double-stranded DNA in a nanopore. *Phys. Rev. Lett.* 90:238101
75. Keyser UF, Koeleman BN, Van Dorp S, Krapf D, Smeets RMM, et al. 2006. Direct force measurements on DNA in a solid-state nanopore. *Nat. Phys.* 2:473–77
76. Hornblower B, Coombs A, Whitaker RD, Kolomeisky A, Picone SJ, et al. 2007. Single-molecule analysis of DNA-protein complexes using nanopores. *Nat. Methods* 4:315–17
77. Bates M, Burns M, Meller A. 2003. Dynamics of DNA molecules in a membrane channel probed by active control techniques. *Biophys. J.* 84:2366–72
78. Baldazzi V, Bradde S, Cocco S, Marinari E, Monasson R. 2007. Inferring DNA sequences from mechanical unzipping data: the large-bandwidth case. *Phys. Rev. E* 75:011904
79. Movileanu L, Schmittschmitt JP, Scholtz JM, Bayley H. 2005. Interactions of peptides with a protein pore. *Biophys. J.* 89:1030–45
80. Stefureac R, Long YT, Kraatz HB, Howard P, Lee JS. 2006. Transport of α-helical peptides through α-hemolysin and aerolysin pores. *Biochemistry* 45:9172–79
81. Ascenzi P, Visca P, Ippolito G, Spallarossa A, Bolognesi M, Montecucco C. 2002. Anthrax toxin: a tripartite lethal combination. *FEBS Lett.* 531:384–88
82. Oukhaled G, Mathe J, Biance AL, Bacri L, Betton JM, et al. 2007. Unfolding of proteins and long transient conformations detected by single nanopore recording. *Phys. Rev. Lett.* 98:158101
83. Oukhaled AG, Bacri L, Mathe J, Pelta J, Auvray L. 2008. Effect of the screening on the transport of polyelectrolytes through nanopores. *Europhys. Lett.* In press
84. Ambjornsson T, Apell SP, Konkoli Z, Di Marzio EA, Kasianowicz JJ. 2002. Charged polymer membrane translocation. *J. Chem. Phys.* 117:4063–73
85. Han AP, Schurmann G, Mondin G, Bitterli RA, Hegelbach NG, et al. 2006. Sensing protein molecules using nanofabricated pores. *Appl. Phys. Lett.* 88:093901
86. Fologea D, Ledden B, McNabb DS, Li J. 2007. Electrical characterization of protein molecules by a solid-state nanopore. *Appl. Phys. Lett.* 91:053901
87. Murphy RJ, Muthukumar M. 2007. Threading synthetic polyelectrolytes through protein pores. *J. Chem. Phys.* 126:051101
88. de Gennes PG. 1999. Problems of DNA entry into a cell. *Physica A* 274:1–7
89. de Gennes PG. 1999. Passive entry of a DNA molecule into a small pore. *Proc. Natl. Acad. Sci. USA* 96:7262–64
90. Muthukumar M. 1999. Polymer translocation through a hole. *J. Chem. Phys.* 111:10371–74
91. Sung W, Park PJ. 1996. Polymer translocation through a pore in a membrane. *Phys. Rev. Lett.* 77:783–86
92. Lubensky DK, Nelson DR. 1999. Driven polymer translocation through a narrow pore. *Biophys. J.* 77:1824–38
93. Sebastian KL, Paul AKR. 2000. Kramers problem for a polymer in a double well. *Phys. Rev. E* 62:927–39

94. Sebastian KL. 2000. Kink motion in the barrier crossing of a chain molecule. *Phys. Rev. E* 61:3245–48
95. Lee S, Sung WY. 2001. Coil-to-stretch transistion, kink formation and efficient barrier crossing of a flexible chain. *Phys. Rev. E* 63:021115
96. Dudko OK, Hummer G, Szabo A. 2006. Intrinsic rates and activation free energies from single-molecule pulling experiments. *Phys. Rev. Lett.* 96:108101
97. Dudko OK, Mathe J, Szabo A, Meller A, Hummer G. 2007. Extracting kinetics from single-molecule force spectroscopy: nanopore unzipping of DNA hairpins. *Biophys. J.* 92:4188–95
98. Kotsev S, Kolomeisky AB. 2006. Effect of orientation in translocation of polymers through nanopores. *J. Chem. Phys.* 125:084906
99. Kong CY, Muthukumar M. 2002. Modeling of polynucleotide translocation through protein pores and nanotubes. *Electrophoresis* 23:2697–703
100. Kong CY, Muthukumar M. 2004. Polymer translocation through a nanopore. II. Excluded volume effect. *J. Chem. Phys.* 120:3460–66
101. Muthukumar M. 2001. Translocation of a confined polymer through a hole. *Phys. Rev. Lett.* 86:3188–91
102. Muthukumar M. 2002. Theory of sequence effects on DNA translocation through proteins and nanopores. *Electrophoresis* 23:1417–20
103. Baldazzi V, Cocco S, Marinari E, Monasson R. 2006. Interference of DNA sequences from mechanical unzipping: an ideal case study. *Phys. Rev. Lett.* 96:128102
104. Aksimentiev A, Schulten K. 2005. Imaging α-hemolysin with molecular dynamics: ionic conductance, osmotic permeability, and the electrostatic potential map. *Biophys. J.* 88:3745–61
105. Muthukumar M, Kong CY. 2006. Simulation of polymer translocation through protein channels. *Proc. Natl. Acad. Sci. USA* 103:5273–78
106. Aksimentiev A, Heng JB, Timp G, Schulten K. 2004. Microscopic kinetics of DNA translocation through synthetic nanopores. *Biophys. J.* 87:2086–97
107. Gracheva ME, Xiong AL, Aksimentiev A, Schulten K, Timp G, Leburton JP. 2006. Simulation of the electric response of DNA translocation through a semiconductor nanopore-capacitor. *Nanotechnology* 17:622–33
108. Heng JB, Aksimentiev A, Ho C, Marks P, Grinkova YV, et al. 2006. The electromechanics of DNA in a synthetic nanopore. *Biophys. J.* 90:1098–106
109. Heng JB, Aksimentiev A, Ho C, Dimitrov V, Sorsch TW, et al. 2005. Beyond the gene chip. *Bell Labs Tech. J.* 10:5–22
110. Zhao Q, Sigalov G, Dimitrov V, Dorvel B, Mirsaidov U, et al. 2007. Detecting SNPs using a synthetic nanopore. *Nano Lett.* 7:1680–85
111. Barcilon V. 1992. Ion flow through narrow membrane channels. 1. *SIAM J. Appl. Math.* 52:1391–404
112. Barcilon V, Chen DP, Eisenberg RS. 1992. Ion flow through narrow membrane channels. 2. *SIAM J. Appl. Math.* 52:1405–25
113. Eisenberg RS. 1996. Computing the field in proteins and channels. *J. Membr. Biol.* 150:1–25

114. Graf P, Kurnikova MG, Coalson RD, Nitzan A. 2004. Comparison of dynamic lattice Monte Carlo simulations and the dielectric self-energy Poisson-Nernst-Planck continuum theory for model ion channels. *J. Phys. Chem. B* 108:2006–15
115. Coalson RD, Kurnikova MG. 2005. Poisson-Nernst-Planck theory approach to the calculation of current through biological ion channels. *IEEE Trans. Nanobiosci.* 4:81–93
116. Mamonov AB, Coalson RD, Nitzan A, Kurnikova MG. 2003. The role of the dielectric barrier in narrow biological channels: a novel composite approach to modeling single-channel currents. *Biophys. J.* 84:3646–61
117. Shilov IY, Kurnikova MG. 2003. Energetics and dynamics of a cyclic oligosaccharide molecule in a confined protein pore environment. a molecular dynamics study. *J. Phys. Chem. B* 107:7189–201
118. Doyle DA, Cabral JM, Pfützner RA, Kuo AL, Gulbis JM, et al. 1998. The structure of the potassium channel: molecular basis of K^+ conduction and selectivity. *Science* 280:69–77
119. Nguyen TL. 2004. Three-dimensional model of the pore form of anthrax protective antigen: structure and biological implications. *J. Biomol. Struct. Dyn.* 22:253–65
120. Di Marzio EA, Kasianowicz JJ. 2003. Phase transitions within the isolated polymer molecule: coupling of the polymer threading a membrane transition to the helix-random coil, the collapse, the adsorption, and the equilibrium polymerization transitions. *J. Chem. Phys.* 119:6378–87
121. Shenoy DK, Barger W, Singh A, Panchal RG, Misakian M, et al. 2005. Functional reconstitution of ion channels in polymerizable lipid membranes. *Nano Lett.* 5:1181–85

Annual Review of Analytical Chemistry

Volume 1, 2008

Contents

A Personal Journey of Discovery: Developing Technology and Changing Biology
Lee Hood 1

Spectroscopic and Statistical Techniques for Information Recovery in Metabonomics and Metabolomics
John C. Lindon and Jeremy K. Nicholson 45

Mass Spectrometry for Rapid Characterization of Microorganisms
Plamen A. Demirev and Catherine Fenselau 71

Scanning Electrochemical Microscopy
Shigeru Amemiya, Allen J. Bard, Fu-Ren F. Fan, Michael V. Mirkin, and Patrick R. Unwin 95

Novel Detection Schemes of Nuclear Magnetic Resonance and Magnetic Resonance Imaging: Applications from Analytical Chemistry to Molecular Sensors
Elad Harel, Leif Schröder, and Shoujun Xu 133

Chemical Cytometry: Fluorescence-Based Single-Cell Analysis
Daniella Cohen, Jane A. Dickerson, Colin D. Whitmore, Emily H. Turner, Monica M. Palcic, Ole Hindsgaul, and Norman J. Dovichi 165

Chemical Analysis of Single Cells
Laura M. Borland, Sumith Kottegoda, K. Scott Phillips, and Nancy L. Allbritton 191

Ion Chemistry in the Interstellar Medium
Theodore P. Snow and Veronica M. Bierbaum 229

Plasma Diagnostics for Unraveling Process Chemistry
Joshua M. Stillahn, Kristina J. Trevino, and Ellen R. Fisher 261

Biomolecule Analysis by Ion Mobility Spectrometry
Brian C. Bohrer, Samuel I. Merenbloom, Stormy L. Koeniger, Amy E. Hilderbrand, and David E. Clemmer 293

In Vitro Electrochemistry of Biological Systems
Kelly L. Adams, Maja Puchades, and Andrew G. Ewing 329

Current Applications of Liquid Chromatography/Mass Spectrometry in Pharmaceutical Discovery After a Decade of Innovation
Bradley L. Ackermann, Michael J. Berna, James A. Eckstein, Lee W. Ott, and Ajai K. Chaudhary 357

Optical Probes for Molecular Processes in Live Cells
Yoshio Umezawa 397

Cell Culture Models in Microfluidic Systems
Ivar Meyvantsson and David J. Beebe 423

Peptides in the Brain: Mass Spectrometry–Based Measurement Approaches and Challenges
Lingjun Li and Jonathan V. Sweedler 451

Analysis of Atmospheric Aerosols
Kimberly A. Prather, Courtney D. Hatch, and Vicki H. Grassian 485

Multiplexed Spectroscopic Detections
Kyle D. Bake and David R. Walt 515

Terrestrial Analysis of the Organic Component of Comet Dust
Scott A. Sandford 549

High-Resolution Mass Spectrometers
Alan G. Marshall and Christopher L. Hendrickson 579

Surface-Enhanced Raman Spectroscopy
Paul L. Stiles, Jon A. Dieringer, Nilam C. Shah, and Richard P. Van Duyne 601

Time-Resolved Microdialysis for In Vivo Neurochemical Measurements and Other Applications
Kristin N. Schultz and Robert T. Kennedy 627

Applications of Ultrafast Lasers for Optical Measurements in Combusting Flows
James R. Gord, Terrence R. Meyer, and Sukesh Roy 663

Matrix-Assisted Laser Desorption/Ionization Imaging Mass Spectrometry for the Investigation of Proteins and Peptides
Kristin E. Burnum, Sara L. Frappier, and Richard M. Caprioli 689

Formation and Characterization of Organic Monolayers on Semiconductor Surfaces
Robert J. Hamers 707

Nanoscopic Porous Sensors
John J. Kasianowicz, Joseph W.F. Robertson, Elaine R. Chan, Joseph E. Reiner, and Vincent M. Stanford 737

Combining Self-Assembled Monolayers and Mass Spectrometry for Applications in Biochips
Zachary A. Gurard-Levin and Milan Mrksich 767

Liposomes: Technologies and Analytical Applications
Aldo Jesorka and Owe Orwar 801

Fundamentals of Protein Separations: 50 Years of Nanotechnology, and Growing
David A. Egas and Mary J. Wirth 833

Functional and Spectroscopic Measurements with Scanning Tunneling Microscopy
Amanda M. Moore and Paul S. Weiss 857

Coherent Anti-Stokes Raman Scattering Microscopy: Chemical Imaging for Biology and Medicine
Conor L. Evans and X. Sunney Xie 883